Intersystem Crossing Processes in Nonplanar Aromatic Heterocyclic Molecules

Karin Schmidt,*,† Sergio Brovelli,‡ Veaceslav Coropceanu,† David Beljonne,†,§ Jérôme Cornil,†,§ Cristina Bazzini,|| Tullio Caronna,|| Riccardo Tubino,‡ Francesco Meinardi,‡ Zhigang Shuai,⊥ and Jean-Luc Brédas*,†

School of Chemistry and Biochemistry and Center of Organic Photonics and Electronics, Georgia Institute of Technology, Atlanta, Georgia 30332-0400, CNISM e Dipartimento di Scienza dei Materiali, Università di Milano Bicocca, Via Cozzi 53, I-20125 Milano, Italy, Service de Chimie des Matériaux Nouveaux, Centre de Recherche en Electronique et Photonique Moléculaires, Université de Mons-Hainaut, B-7000 Mons, Belgium, Dipartimento di Chimica Industriale della Facoltà di Ingegneria, Università di Bergamo, Viale Marconi 5, I-24044 Dalmine (BG), Italy, and Key Laboratory of Organic Solids, Institute of Chemistry, The Chinese Academy of Sciences, 100080 Beijing, P. R. China

Received: July 5, 2007

A comprehensive study of the photophysical properties of a series of monoaza[5]helicenes is presented on the basis of joint optical spectroscopy and quantum chemistry investigations. The molecules have been characterized by absorption and CW/time-resolved luminescence measurements. All quantities related to spin−orbit-coupling processes, such as intersystem crossing rates and radiative phosphorescence lifetimes, were found to depend strongly on the nitrogen position within the carbon backbone. Density functional theory and semiempirical quantum-chemical methods were used to evaluate the molecular geometries, the characteristics of the excited singlet and triplet states, and the spin−orbit coupling matrix elements. We demonstrate that the magnitude of spin−orbit coupling is directly correlated with the degree of deviation from planarity. The trends from the calculated photophysical quantities, namely, radiative fluorescence and phosphorescence decay rates and intersystem crossing rates, of the mono-aza-helicenes are fully consistent with experiment.

I. Introduction

Among the families of condensed aromatic molecules, helicenes occupy a peculiar position. Helicenes consist of fused rings that arrange themselves in a nonplanar fashion as a result of steric hindrances. Thus, they combine the characteristics of a conjugated π-electron system with nonplanarity, which is known to trigger spin−orbit coupling. These systems generally exhibit larger intersystem crossing rates[1−3] and larger magnetic dipole moments[4,5] than their planar analogs.

In this work, we focus on the mono-aza derivatives of [5]-helicene (H5). The chemical structure of [5]helicene and the positions of the nitrogen-substitution sites are illustratred in Figure 1. Several aza-[5]helicenes bearing one or two nitrogen atoms in selected positions have recently been synthesized and characterized.[6,7] It has been shown that the position of the nitrogen atom(s) has an important effect on the structural and spectroscopic properties of the molecules. For instance, as will be illustrated below for monoaza[5]helicenes, the relative phosphorescence/fluorescence ratio can be markedly tuned by changing the position of the N atom. The interplay between phosphorescence and fluorescence is determined by several nonradiative processes, including intersystem crossing (ISC).

Spin−orbit coupling (SOC) mediates the excitation transfer between singlet and triplet states and is central to the work presented here. Processes associated with spin−orbit coupling in aromatic compounds of aza-helicene type are expected to be influenced by two major contributions. On one hand, departure from coplanarity is considered to be responsible for the enhancement of ISC observed in [*n*]helicenes from $n = 3$ to $n = 7$ rings, whose luminescence properties, including phosphorescence, have been comprehensively studied;[8−14] the ISC rates observed in oligo(phenylene ethynylene)s and oligothiophenes were also shown to originate from nonplanarity of the molecules.[2] According to Sapir and Vander Donckt,[1] the intersystem crossing rates for H5 are intrinsically larger than those for planar phenanthrene. On the other hand, the introduction of a heteroatom such as nitrogen is well-known to significantly enhance intersystem crossing in coplanar molecules [e.g., in studies of (di-)aza-benzene-, -naphthalene-, and −phenanthrene derivatives[15−20]); this arises from a very effective spin−orbit coupling between

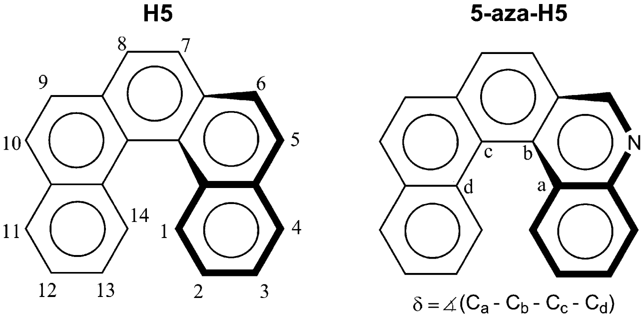

Figure 1. Chemical structure and atomic labels of [5]helicene (H5) and the monoaza[5]helicenes with 5-aza-[5]helicene taken as representative.

---

* To whom correspondence should be addressed. E-mail: karin.schmidt@chemistry.gatech.edu (K.S.), jean-luc.bredas@chemistry.gatech.edu (J.-L.B.).

† Georgia Institute of Technology.

‡ Università di Milano Bicocca.

§ Université de Mons-Hainaut.

|| Università di Bergamo.

⊥ The Chinese Academy of Sciences.

10.1021/jp075248q CCC: $37.00

low-lying $n-\pi^*$ states (i.e., transitions involving an orbital containing the nitrogen lone pair) and $\pi-\pi^*$ states.

Thus, the question arises as to which of these two effects is mainly responsible for the impact of the heteroatom position on the measured photophysical properties. Judging from the findings on small nitrogen-heterocyclic molecules and [*n*]-helicenes, we anticipate a subtle interplay to occur between SOC among $\pi-\pi^*$ singlet and triplet states and SOC among $n-\pi^*$ and $\pi-\pi^*$ states.

The recent development of TD-DFT-based excited-state geometry optimizations[21,31c] makes available a very promising methodology to characterize excited states at the *first-principles* level. Furthermore, a variety of promising ab initio (MRMP,[22a,b] EOM-CC[22c]) and DFT-based (MRCI-DFT,[22d] TD-DFT//QR[22e−h]) methods are currently emerging in the literature to characterize the excited states and related system properties, such as SOC or the nonlinear optical response. However, at present, they are not routinely applied and have been thoroughly benchmarked only with respect to specific problems or rather small systems. Therefore, considering that the performance of the semiempirical INDO/S Hamiltonian is very well documented and known to yield reliable results for a broad variety of compounds and a wide range of properties (particularly for those requiring excited states; see, e.g., ref 22i), we have chosen to evaluate the SOC matrix elements on the basis of INDO/CIS; in particular, we note that INDO/CIS//SOC has been previously applied successfully to study ISC processes in oligo(phenylene ethynylene)s and oligothiophenes.[2] In this work, we use this approach (i) to address each individual transition process, i.e., absorption, fluorescence, intersystem crossing, and phosphorescence, in the appropriate molecular conformation and (ii) to evaluate the influence of the nitrogen position within the helicene backbone.

This article is structured as follows: Section II provides a description of our techniques and a brief review of the theoretical background for spin−orbit coupling and intersystem crossing. In section III, we discuss a first series of results regarding the impact of the presence of the nitrogen atom and its position on molecular geometries and photophysical quantities such as singlet transition energies, oscillator strengths, and fluorescence decay rates. This will allow a thorough characterization of the lowest singlet excited states. In section IV, we turn to a discussion of theoretical results for spin−orbit coupling (including its sensitivity with respect to the molecular geometry), vibrational coupling between singlet and triplet states, and intersystem crossing rates; the calculated and measured ISC rates are compared in light of the phosphorescence lifetimes.

II. Methodology

(a) Experimental Details. Different strategies have been followed to prepare [5]helicene and all the possible monosubstituted aza derivatives, as described in ref 6. Solutions of these molecules were prepared in ethanol at a concentration of 10^{-6} mol/L or lower. The recording procedure for the absorption and luminescence spectra is described elsewhere.[23] Singlet and triplet photoluminescence spectra were successively merged using the proper renormalization factor R_{PF}. At room temperature, the emission intensity of the triplet was below the detection limit regardless of the detection technique.

The photoluminescence quantum yields (Φ_S) were measured using a relative method for optical dilute solutions, using as a reference the quantum yield of quinine sulfate dehydrate in 1.0 N sulfuric acid ($\sim 10^{-5}$ M; $\Phi_S = 0.546 \pm 5\%$).[24] The fluorescence emission signal was recorded synchronously with the excitation lamp in order to eliminate the contributions due to impurities and precursors. The quantum yields were measured at room temperature for an excitation wavelength of 365 nm. The error on Φ_S values is about 10−20%. All spectra were corrected for the instrument spectral response, which was measured with a calibrated lamp and tested with a 0.105 M $HClO_4$ quinine sulfate dihydrate solution.[24]

Fluorescence time-resolved measurements (τ^{S}_{tot}) were performed with a streak-camera-based setup with a temporal resolution better than 100 ps by exciting the solutions with the second harmonic of a Ti:sapphire laser. Phosphorescence lifetimes, τ^{T}_{tot}, were measured with the decay tool of the Varian Eclipse Spectrofluorimeter with a temporal resolution of 0.01 s. It must be noted that processes such as photocyclization and photo-oxidation can be invoked as a result of exposure to the laser during the measurement. The photocyclization of [5]-helicene, extensively studied by Palewska et al.[10] and Grellmann et al.,[25] for example, imposes a complication in recording the emission spectra, as the formation of dihydrobenzoperylene is a pathway competing with both fluorescence and phosphorescence. Such mechanisms have to be anticipated for the monoaza-[5]helicenes as well. Before and after each of the time-resolved measurements, integrated spectra were recorded to check whether the shape of the spectra was kept or showed evidence of deterioration. In cases where deterioration became evident, the sample was replaced by a freshly prepared solution, and the laser power was reduced. Remaining effects not detectable in CW mode could, however, have an impact on the final data, leading to an error of about 0.1−0.2 ns.

The nonradiative contributions to the decay of the fluorescence signal are intersystem crossing and the direct nonradiative relaxation from the lowest excited state S_1 into the singlet ground state

$$k^{S}_{\mathrm{nonrad-S}} = k_{\mathrm{ISC}} + k^{S}_{\mathrm{nonrad-S_0}} = (1 - \Phi_S)k^{S}_{\mathrm{tot}} \qquad (1)$$

Because the total fluorescence lifetimes were found in the experiment to be temperature-independent, the purely singlet-related nonradiative decay rate can be assumed to be negligible ($k^{S}_{\mathrm{nonrad-S_0}} \ll k_{\mathrm{ISC}}$), and an upper-limit estimate for the intersystem crossing rate can be given by

$$k_{\mathrm{ISC}} = (1 - \Phi_S)k^{S}_{\mathrm{tot}} \qquad (2)$$

(b) Computational Details and Theoretical Background. *Geometry Optimizations.* We performed geometry optimizations for the ground (S_0) and excited states (S_1 and T_1) of all molecules, followed by calculations of harmonic vibrational frequencies and normal modes. The S_0 and T_1 states were described at the restricted and unrestricted density functional theory (DFT) levels, respectively. The geometries of the excited singlet S_1 states were obtained from time-dependent DFT (TD-DFT)[26−28] calculations. In all cases, the B3LYP exchange-correlation functional[29] and the split valence SV(P) basis set[30] were used as implemented in the TURBOMOLE package.[31] For the sake of comparison, we also computed the geometries and vibrational modes using the semiempirical AM1[32] method in combination with a configuration interaction (AM1/CI) scheme as implemented in the AMPAC package.[33] For [5]helicene, the calculations were performed both with and without the imposition of symmetry constraints.

Excited-State Properties. The vertical transition energies and the properties of the singlet and triplet excited states were calculated with TD-DFT[26,27] [B3LYP/SV(P)] and the semiempirical INDO/CIS method[34] combined with a single configura-

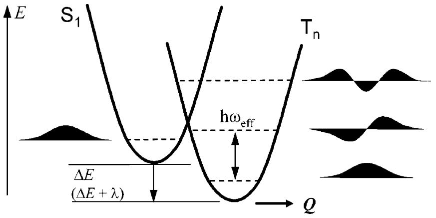

Figure 2. Schematic illustration of the displaced potential energy surfaces corresponding to the singlet S_1 state and a triplet state T_n ($n \geq 1$) and definition of the parameters in eq 10. Also illustrated are the shapes of the vibrational wavefunctions, corresponding to the effective normal mode ω, whose overlap gives rise to the Franck–Condon-like density of states.

TABLE 1: (0–0) Transition Energies (eV) Determined from the $S_0 \rightarrow S_1$ Absorption Spectra (298 K) and $S_1 \rightarrow S_0$ and $T_1 \rightarrow S_0$ Emission Spectra (77 K) in Ethanol

	singlet		triplet
compound	E_{abs} (eV)	E_{em} (eV)	E_{phos} (eV)
H5	3.13	–	2.45
1-aza-H5	3.13	3.10	2.48
2-aza-H5	3.03	–	2.42
3-aza-H5	3.05	3.04	2.47
4-aza-H5	3.14	3.11	2.45
5-aza-H5	3.13	3.10	2.47
6-aza-H5	3.14	3.11	2.45
7-aza-H5	3.10	3.04	2.44

tion interaction (CIS) scheme (INDO/CIS). The electron–electron interactions in INDO/CIS were described with the Ohno–Klopman potential;[35] this potential has been shown to describe better the S_0–T_1 energy difference in oligo(phenylene)s, oligothiophenes, and oligofluorenes than the more commonly applied Mataga–Nishimoto potential.[36,37] The CI active space involved 35 occupied and 35 unoccupied orbitals to ensure that the relevant π- and σ-type orbitals were taken into account in the description of the lowest excited states of the nonplanar compounds.

Spin–Orbit Coupling. In organic systems, spin–orbit coupling is considered to be a small correction to purely nonrelativistic electronic states. The spin–orbit Hamiltonian in central-field approximation is written as[15]

$$\hat{H}_{so} = \alpha_F{}^2 \sum_{\mu}^{N} \sum_{i}^{n} \frac{Z_\mu}{r_{i\mu}{}^3} \vec{L}_i \vec{S}_i \tag{3}$$

where α_F is the fine-structure constant; Z is the effective nuclear charge at nucleus μ; and S and L are the spin and orbital angular momenta of electron i, respectively. The computation of the expectation values associated with the SOC Hamiltonian follows the formalism described in refs 2, 15, and 38.

The expectation value for the spin–orbit coupling is expressed in the framework of first-order perturbation theory as

$$\langle {}^1\Psi^{(0)}|\hat{H}_{so}|{}^3\Psi^{(0)}\rangle = \alpha_F{}^2 \sum_{\mu}^{N} \sum_{i}^{n} \left\langle \frac{Z_\mu}{r_{i\mu}^3}\, {}^1\psi^{(0)}|\vec{L}_i|{}^3\psi^{(0)} \right\rangle \times \left\langle \frac{1}{\sqrt{2}}(\alpha\beta - \beta\alpha)|\vec{S}| \begin{bmatrix} \alpha\alpha \\ \frac{1}{\sqrt{2}}(\alpha\beta + \beta\alpha) \\ \beta\beta \end{bmatrix} \right\rangle \tag{4}$$

where ${}^1\Psi^{(0)}$ (${}^1\psi^{(0)}$) and ${}^3\Psi^{(0)}$ (${}^3\psi^{(0)}$) are the total (spatial) electronic wavefunctions of the singlet and triplet states, respectively, in the undisturbed system. The energies and wavefunctions of the singlet and triplet excited states were obtained from the INDO/CIS calculations.

Fluorescence and Phosphorescence Lifetimes. The rate of a spontaneous radiative transition such as fluorescence or phosphorescence in the gas phase is described by the Einstein coefficient

$$A = \frac{(E_1 - E_0)^3}{3\epsilon_0 \pi \hbar^4 c^3} |\vec{\mu}_{1\rightarrow 0}|^2 \tag{5}$$

where E_1 and E_0 are the energies of the excited and ground states, respectively, and $\vec{\mu}_{1\rightarrow 0}$ is the corresponding transition dipole moment. In the case of the fluorescence decay rate k^S_{rad}, the transition dipole moment $\vec{\mu}_{S_1\rightarrow S_0}$ and the S_1 vertical transition energy (from the relaxed S_1 geometry) were inserted.

The radiative transition between the lowest triplet state and the ground state gives rise to a T_1–S_0 phosphorescence signal. The corresponding radiative decay rate k^T_{rad} is one component of the overall triplet decay rate k^T_{tot}

$$k^T_{tot} = \frac{1}{\tau^T_{tot}} = k^T_{rad} + k^T_{nonrad} \tag{6}$$

As a consequence of the spin–orbit interaction, each state of predominant singlet character acquires a certain amount of triplet admixture and vice versa. Formulated in the framework of first-order perturbation theory, the radiative transition probability k^T_{rad} between T_1 and S_0 is proportional to the transition dipole moment $\vec{\mu}_{T_1\rightarrow S_0}$ squared[16]

$$\begin{aligned} \vec{\mu}_{T_1\rightarrow S_0} &= \langle {}^3\Psi_1|\vec{\mu}|{}^1\Psi_0\rangle \\ &= \sum_k \frac{\langle \Psi_1^{3(0)}|\hat{H}_{SO}|\Psi_k^{1(0)}\rangle}{{}^3E_1 - {}^1E_k} \times \vec{\mu}_{S_k\rightarrow S_0} \\ &\quad + \sum_m \frac{\langle \Psi_m^{3(0)}|\hat{H}_{SO}|\Psi_0^{1(0)}\rangle}{{}^3E_m - {}^1E_0} \times \vec{\mu}_{T_m\rightarrow T_1} \end{aligned} \tag{7}$$

where the summation k runs over all singlet states and the summation m runs over all triplet states. We computed the transition dipole moment by inserting into eq 7 the individual S_0–S_n and T_1–T_n transition dipole moments and the SOC matrix elements obtained from eq 4.

Intersystem Crossing Rates. The decay rate of the population in state S_n due to intersystem crossing to any state T_m is given by

$$k^n_{ISC} = \sum_m k^{nm}_{ISC} \tag{8}$$

Each individual ISC channel was treated as a nonradiative transition between S_n and T_m, expressed by the Fermi Golden Rule[39,40]

$$k^{nm}_{ISC} = \frac{2\pi}{\hbar} \langle \Psi_n^{1(0)}|\hat{H}_{SO}|\Psi_m^{3(0)}\rangle^2 \times \text{FCWD} \tag{9}$$

Throughout our work, it is assumed that the relaxation via internal conversion into the lowest excited singlet state S_1 is fast enough so that intersystem crossing essentially proceeds from S_1. This assumption is supported experimentally by the absence of any rise time of the fluorescence signals. However, ISC contributions associated with higher-lying singlet states can

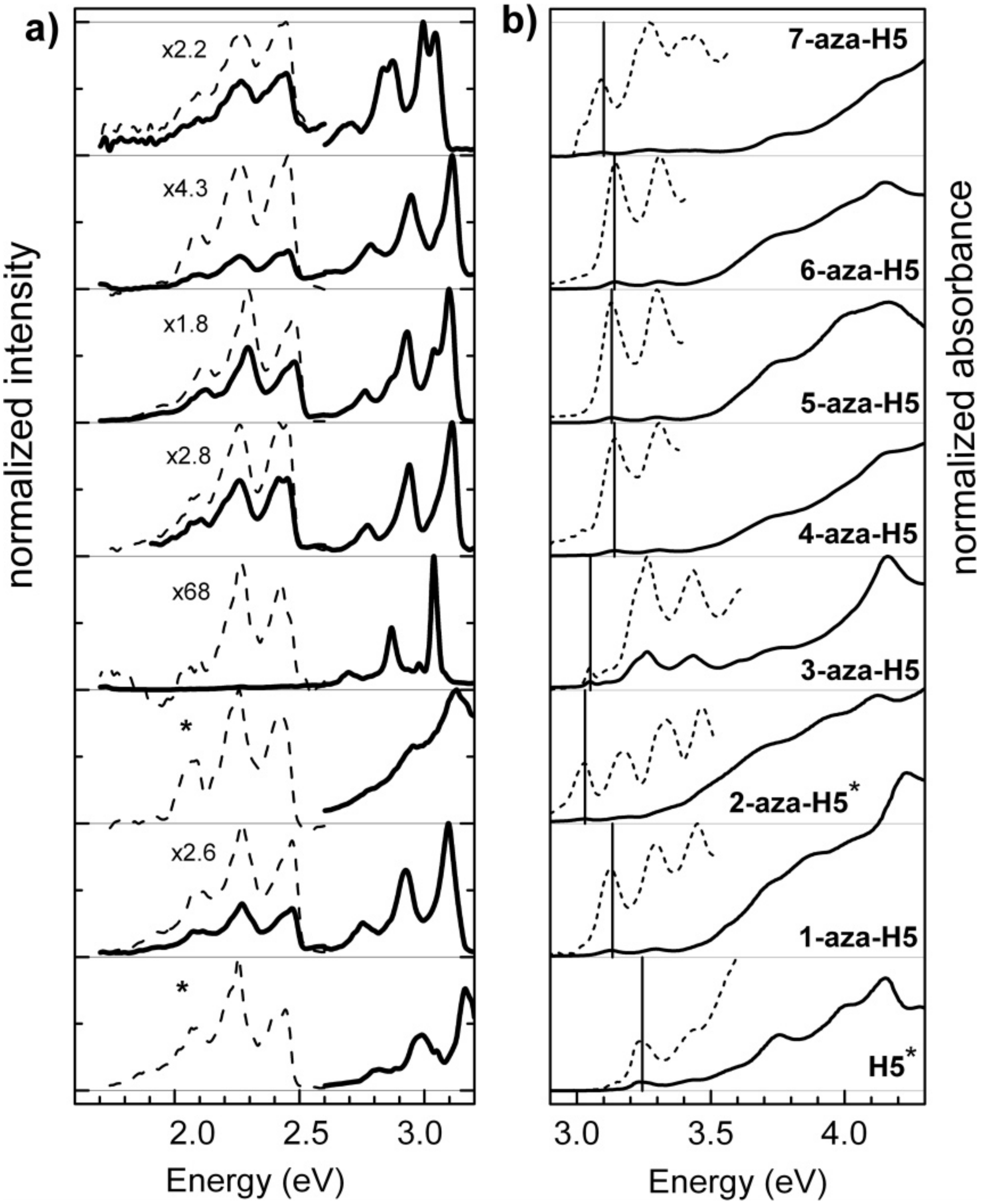

Figure 3. (a) Emission spectra of H5 and the monoaza-H5 series in ethanol at 77 K. In addition, the normalized phosphorescence spectra are shown (dashed lines). Asterisks indicate compounds for which the phosphorescence to fluorescence ratio could not be obtained. (b) Low-energy portion of the absorption of H5 and the monoaza[5]helicene series recorded at 298 K in ethanol (solid lines). The weak features at the absorption onset have been enlarged (dashed lines). In the enlarged 2-aza-H5 spectrum (dashed), the strong shoulder at ca. 3.75 eV has been removed to highlight the fine structure of lower transitions. The vertical bars indicate the position of the absorption onset.

be added by weighting their formal rates k^n_{ISC} by their Boltzmann-distributed population $\sim\exp[(E_n - E_1)/k_\mathrm{B}T]$, where T is the temperature and k_B is the Boltzmann constant.

Two independent contributions enter the decay rate: (i) the SOC coupling matrix element squared (computed according to eq 4) and (ii) the Franck−Condon-weighted density of states (FCWD) that ensures energy conservation. The latter was evaluated in the framework of Marcus−Levich−Jortner theory[41]

$$\mathrm{FCWD} = \frac{1}{\sqrt{4\pi\lambda k_\mathrm{B}T}} \sum_{n=0}^{\infty} \exp(-S)\frac{S^n}{n!}\exp\left[-\frac{(\Delta E + n\hbar\omega + \lambda)^2}{4\lambda k_\mathrm{B}T}\right] \quad (10)$$

Here, λ is the Marcus reorganization energy (due to intramolecular, low-frequency vibrations, λ_L, and solvent-induced relaxation, λ_S), ΔE is the difference between the energies of S_1 and the triplet state at their equilibrium geometry (see Figure 2), $\hbar\omega$ is the energy of an effective nonclassical vibrational mode involved in the transition, and S is the associated Huang−Rhys factor.

To estimate the *intramolecular* contribution to parameter λ and to determine the effective high-energy vibration, we optimized the geometries of all triplet excited states with energies in resonanance with or lower than S_1; the corresponding normal vibrational modes were computed at the AM1/CI level (note that the geometry and the vibrations in the S_1 state were

TABLE 2: Energies of the Lowest Excited Singlet and Triplet States (eV) and Oscillator Strengths for the S_0−Singlet Transitions in [5]Helicene and in the Monoaza Derivatives Determined with INDO/CIS for Different Geometries

		S_0 geometry			S_1 geometry			T_1 geometry
		singlet		triplet	singlet		triplet	triplet
compound		*E* (eV)	*f*	*E* (eV)	*E* (eV)	*f*	*E* (eV)	*E* (eV)
H5	1	3.44	0.0114	2.03	3.16	0.0003	1.79	1.50
	2	3.47	0.0001	2.49	3.19	0.0079	2.35	2.20
	3	4.03	0.0010	2.95	3.88	0.0068	2.74	2.80
1-aza-H5	1	3.47	0.0203	2.08	–	–	–	1.52
	2	3.48	0.0218	2.58	–	–	–	2.30
	3	4.01	0.1609	2.95	–	–	–	2.84
2-aza-H5	1	3.46	0.0220	2.06	3.17	0.0125	1.83	1.54
	2	3.48	0.0027	2.57	3.21	0.0038	2.41	2.27
	3	4.04	0.0671	2.96	3.88	0.0694	2.73	2.84
3-aza-H5	1	3.47	0.0263	2.07	3.17	0.0202	1.83	1.52
	2	3.48	0.0055	2.55	3.23	0.0095	2.40	2.22
	3	4.05	0.0153	2.96	3.90	0.0124	2.72	2.76
4-aza-H5	1	3.46	0.0079	2.07	3.17	0.0088	1.83	1.51
	2	3.48	0.0126	2.58	3.22	0.0074	2.43	2.31
	3	3.99	0.1364	2.96	3.81	0.2161	2.75	2.83
5-aza-H5	1	3.46	0.0226	2.10	3.17	0.0316	1.89	1.54
	2	3.51	0.0073	2.55	3.26	0.0030	2.44	2.43
	3	4.02	0.0833	2.94	3.85	0.1403	2.72	2.79
6-aza-H5	1	3.47	0.0289	2.10	3.17	0.0376	1.86	1.56
	2	3.50	0.0272	2.56	3.24	0.0131	2.40	2.25
	3	4.01	0.1521	2.97	3.83	0.2238	2.73	2.74
7-aza-H5	1	3.46	0.1131	2.12	3.16	0.1037	1.91	1.54
	2	3.54	0.0088	2.50	3.30	0.0130	2.37	2.22
	3	4.05	0.0137	2.93	3.89	0.0225	2.64	2.71

provided with the same method). The vibrational relaxation energies of the triplet states and the effective mode $\hbar\omega$ with its associated Huang−Rhys factor *S* were determined using the DUSHIN program developed by Reimers.[42]

III. Results and Discussion: Part 1

(a) Geometries. The calculated structural parameters characterizing the ground-state geometry, such as C−C and C−N bond lengths, bond angles, dihedral angles δ, and helix pitch, are in excellent agreement with values previously published.[4,5,10,43] DFT-optimized structures of helicenes have been shown to reliably describe racemization barriers[43] and CD spectra,[4] i.e., quantities that are sensitive to δ and the resulting magnetic moment. Thus, we are confident that additional van der Waals interactions, albeit present, will not affect the overall trends in δ. To monitor the deviation from planarity, we tracked the change in inner dihedral angle δ ($C_a-C_b-C_c-C_d$) (cf. Figure 1) during the relaxation. As reported elsewhere,[23] the dihedral angle exhibits small fluctuations in the ground state throughout the series. The helices maintain a (DFT-optimized) δ value between 28° and 30° that corresponds to a considerable deviation from planarity; these values match the range $\delta_{exp} = 27-33°$ extracted from X-ray diffraction experiments.[5,6,44,45] In the S_1 state, the helices tend to open up (δ increases by some 2°), whereas they flatten (by some 2°) in the T_1 state.[23]

(b) Absorption and Emission Spectra. The absorption spectra recorded for all monoaza[5]helicenes (shown in Figure 3b) share a very weak onset at ∼3.1 eV and a series of much stronger transitions starting beyond 3.7 eV. The electronic transitions into the lowest singlet states and their vibronic replicas are partially obscured by the strongly absorbing state at ∼3.7 eV. For several molecules, i.e., 1- and 4−7-aza-H5, the first electronic transition is sufficiently separated from the onset of the adjacent transition to reveal the first vibronic replica of the $S_0 \rightarrow S_1$ transition.

Closer inspection of the absorption of molecules H5 and 2- and 3-aza-H5 (see Figure 3b) suggests that the low-energy tail of absorption is composed of two close-lying, weakly absorbing states. The positions of the zero-phonon line in the first absorption peak for H5 and all monoaza[5]helicenes are collected in Table 1.

The emission spectra measured at 77 K (see Figure 3a and Table 1) share a consistent pattern throughout the series. The feature at ∼2.45 eV, because of its very long lifetime (≥1 s), is attributed to phosphorescence; the phosphorescence signal is not affected by any impurities. The helicene fluorescence gives rise to a band at ∼3.1 eV (cf. Table 1). For the molecules H5 and 2-aza-H5, which were particularly difficult to purify, an additional fluorescence signal of the precursors (which could not be removed successfully from the material) is observed; this leads to a complicated convolution of the vibronic progressions related to both helicene (3.15−3.2 eV) and precursor (∼3.35 eV) emissions. The purification problems of 2-aza-H5 are attributed to the reaction route that had to be specially designed for this compound; the synthetic route has a very small yield and utilizes three-ring precursors that are difficult to remove. The onsets of the absorption, fluorescence, and phosphorescence bands (Table 1), as well as the respective line shapes, are rather insensitive to the nitrogen substitution site. At room temperature, the phosphorescence vanishes entirely, and the shape of the fluorescence signal is nearly unaffected by the position of the N atom. The INDO/CIS (Table 2) and TD-DFT (Supporting Information) vertical transition energies between S_0 and the lowest singlet and triplet excited states were calculated in the ground-state geometry for absorption and in the relaxed S_1 and T_1 geometries for the case of emission. In the case of absorption, according to INDO/CIS, the two lowest singlet excited states are lying very close in energy with respect to the separation of successive vibronic progression features (ca. 0.17 eV). In agreement with the measured absorption spectra, the transitions into these lowest two singlet states are calculated to be very weak. The TD-DFT results confirm this observation (Supporting Information). Whatever the chosen geometry, the positions of the lowest singlet states and triplet states are nearly

TABLE 3: Fluorescence Parameters at 77 K of the Monoaza[5]helicene Series Recorded in Ethanol

compound	τ^S_{tot} (ns)	Φ_S	τ^S_{rad} (ns)	k_{ISC} (10^8 s^{-1})	k^S_{rad} (10^7 s^{-1})	k^S_{tot} (10^8 s^{-1})
H5[a]	25.5	0.04	637.5	0.38	0.16	0.39
H5[b]	25.0	0.07	357.1	0.37	0.28	0.40
1-aza-H5	3.9	0.06	66.1	2.41	1.51	2.56
3-aza-H5	3.3	0.27	12.2	2.21	8.21	3.03
4-aza-H5	3.6	0.16	22.8	2.34	4.39	2.78
5-aza-H5	4.5	0.20	23.0	1.79	4.36	2.22
6-aza-H5	2.6	0.17	15.0	3.18	6.65	3.85
7-aza-H5	3.4	0.26	13.2	2.19	7.56	2.94

[a] From ref 25. [b] From ref 1.

independent of the variation in nitrogen position (e.g., at the INDO/CIS level with the S_0 geometry, $E_{S1} = 3.44-3.47$ eV, $E_{S2} = 3.47-3.54$ eV, $E_{S3} = 3.93-4.05$ eV).

The INDO/CIS results indicate a reordering of the lowest singlet states in H5 when geometric relaxation is allowed in the excited states. In TD-DFT (Supporting Information), the state ordering remains unchanged with geometry and agrees with earlier findings.[4,11,46] In both INDO/CIS and TD-DFT cases, the *emissive* S_1 state in H5 is classified as 2^1A and S_2 as 1^1B. Geometrical relaxation within S_1 lowers the S_1-S_0 transition energy by ca. 0.3 eV at the INDO/CIS level and ca. 0.25 eV at the TD-DFT level; upon relaxation within the T_1 state, the calculated T_1 state energy is stabilized by 0.52−0.56 eV (INDO/CIS) and 0.6 eV (TD-DFT).

The onsets of the absorption spectra correspond to the (electronic) adiabatic transition energies that are impacted in addition by the difference in zero-point energies, solvent polarization, and stabilization due to coupling to intramolecular low-frequency vibrations. When taking into account the anticipated solvent shifts (the measured solvent-dependent onset of absorption and fluorescence in H5 is scattered within 0.1 eV)[9,11,25,47,48] and the zero-point differences of 82−92 meV (from summation over all normal modes in S_1 and S_0), we found that the calculated adiabatic TD-DFT transition energies (for a complete set of values, see the table in the Supporting Information) tend to overestimate the observed absorption onsets (Table 1) by less than 0.2 eV.

(c) Fluorescence Lifetimes. The total fluorescence lifetimes and fluorescence quantum yields Φ_S are collected in Table 3, together with the corresponding fluorescence decay rates and the intersystem crossing rates (evaluated from eq 2).

The total lifetimes were found to be nearly temperature-independent between 300 and 77 K. This indicates that the activated (phonon-assisted) nonradiative channels, which are expected to be strongly temperature-dependent, are negligible. Because S_1 and S_2 have very small transition dipole moments to S_0 and are close in energy (cf. Table 2), we considered the contribution of both states to the fluorescence rate by summing over the individual, Boltzmann-weighted fluorescence decay rates k^S_{rad} (eq 5) associated with S_1 and S_2. The INDO/CIS- and TD-DFT-calculated total radiative decay rates are shown in Figure 4 (and Table 4 for INDO/CIS) in comparison to the measured k^S_{rad} values.

As can be seen from Figure 4, the calculated values are underestimated with respect to the experimental fluorescence rates at both the TD-DFT and INDO/CIS levels, but are predicted to be of the same order of magnitude by both methods. In general, the overall sensitivity of k^S_{rad} to the N-substitution site is reflected somewhat better with TD-DFT than with INDO/CIS (which predicted a disproportionately large rate for 7-aza-H5). No attempt to correct these rates for the influence of the solvent was made. (We note here that the available solvent models that are commonly used in the literature are deficient in describing the solvent effects on the oscillator strength of weak optical transitions.)

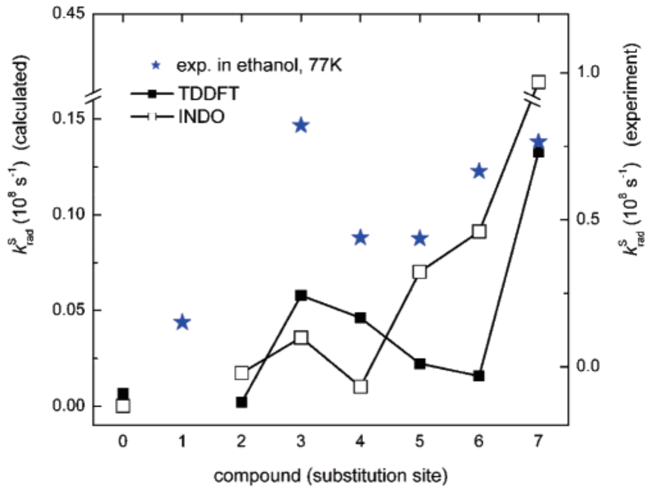

Figure 4. Calculated and experimental radiative fluorescence decay rates of H5 and monoaza[5]helicenes. Note the major break in the axis corresponding to the calculated k^S_{rad}.

TABLE 4: Estimated Fluorescence Decay Rates k^S_{rad} and Intersystem Crossing Rates k_{ISC} from INDO Calculations[a]

	k^S_{rad} (10^6 s^{-1})	k_{ISC} (10^9 s^{-1})			
		$\lambda = 0.1$ eV		$\lambda = 0.2$ eV	
compound	total	77 K	298 K	77 K	298 K
H5	0.02	0.45	0.81	0.34	0.48
2-aza-H5	1.74	0.58	0.93	0.69	0.73
3-aza-H5	3.59	0.11	0.38	0.50	3.67
4-aza-H5	1.03	0.22	0.59	0.28	0.37
5-aza-H5	7.02	0.16	0.37	0.45	0.39
6-aza-H5	9.11	2.08	1.97	0.86	1.27
7-aza-H5	41.76	1.87	1.34	0.85	1.00

[a] ISC rates were estimated using eqs 8−10 for different temperatures and different reorganization energies λ. The effective mode entering eq 10 corresponds to $\hbar\omega = 1600$ cm^{-1} and $S = 0.9$

Note that application of INDO/CIS and TD-DFT is known to be problematic when weakly optically allowed states are involved. The related source of error is the inherent inability of these methods to consider a multiple excitation character in the description of the states, a contribution that might affect k^S_{rad}. To evaluate potential contributions of doubly and more highly excited determinants, in particular, to S_1 and S_2, additional calculations using multireference configuration interaction with singles and doubles (MRD-CI) coupled to the INDO/S Hamiltonian were performed.[49] This method was previously shown to correctly capture the nature of optically forbidden A_g states.[50] The MRD-CI results demonstrate that S_1, S_2, and all triplet states below S_1 can be well described with singly excited determinants.

Among the aza-H5 compounds, both INDO/CIS- and TD-DFT-predicted k^S_{rad} values essentially follow the trend seen in experiment. However, theory cannot resolve the large difference between the aza-H5 compounds and their parent H5. This might be in part related to experimental difficulties in measuring k^S_{rad} and k_{ISC} of H5. Our own efforts to reproduce published values from literature[1,25] failed, because of (i) naphthalene-related precursors with a probably higher oscillator strength that were present (that give rise to unwanted contributions in the PL spectra) and (ii) photocyclization of the helix under UV

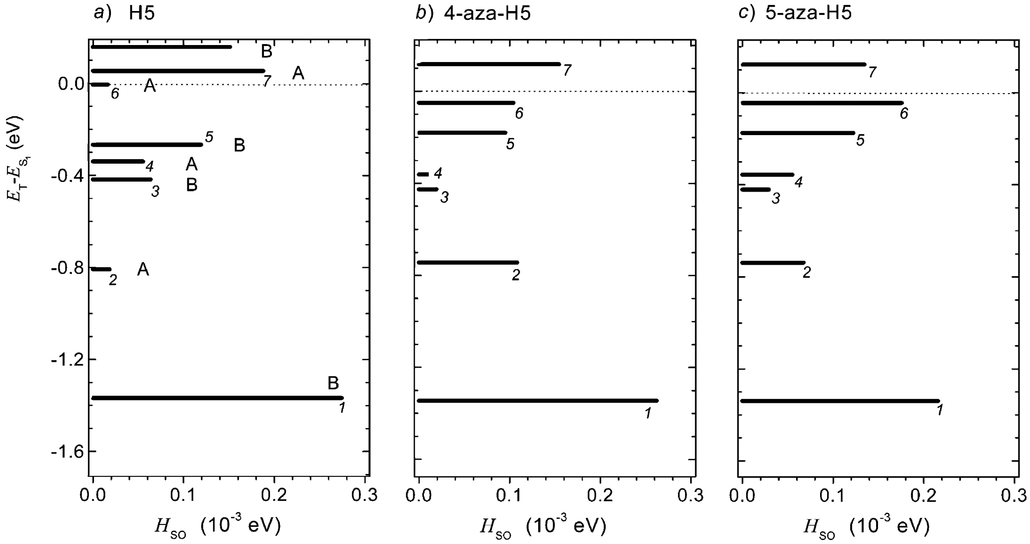

Figure 5. INDO/CIS spin−orbit coupling expectation values between S_1 and T_n for (a) [5]helicene and (b,c) 4-aza- and 5-aza[5]helicenes obtained in the S_1 geometry. The labels refer to the triplet states T_n; additional labels on the states of H5 indicate their symmetry character.

irradiation that would cause a change of the PL spectrum. Considering this experimental uncertainty associated with the acquisition of $k_{\mathrm{rad}}^{\mathrm{S}}$ and k_{ISC} in H5, we will not directly compare these values to the corresponding rates in aza-H5 and to our calculated results.

IV. Results and Discussion: Part 2

(a) Spin−Orbit Coupling. To theoretically describe the intersystem crossing between the singlet and triplet manifolds, the spin−orbit coupling matrix element between all contributing pairs of states and the corresponding Franck−Condon factors must be evaluated. We assumed that, upon excitation, the molecule rapidly relaxes into the S_1 state (via internal conversion), from which SOC gives rise to intersystem crossing. Given the energetic proximity of S_1 and S_2, SOC from S_2 might contribute to ISC as well. Therefore, the spin−orbit coupling from both S_1 and S_2 to the triplet manifold were computed on the basis of the relaxed S_1 geometry.

The SOC coupling values are on the order of 0.01−0.3 meV (∼0.1−3 cm^{-1}), which is the expected range for organic molecules.[51] The coupling observed for the aza compounds is slightly larger than that for the purely hydrocarbon molecule H5, because H_{so} explicitly contains the effective atomic number of the nuclei (hence, nitrogen atoms contribute more than carbon atoms). The coupling between, e.g., S_1 and T_1, shown in Figure 5, is not significantly altered in the aza-H5 series with respect to H5.

The most likely channels for intersystem crossing involve the SOC of the thermally relaxed S_1 state to final triplet states that are either quasiresonant with or energetically *below* S_1. The strongest coupling is observed to (off-resonant) T_1, although T_5 and T_6 also strongly couple to S_1.

It is important to note that we do not observe states with (partial) $n-\pi^*$ character among the lowest excited states regardless of the actual geometry and spin multiplicity considered. According to the INDO/CIS calculations, all triplet states close to resonance with S_1 or located below S_1 and S_1 itself are of $\pi-\pi^*$ character [the T_n ($n \geq 1$) state energies are listed in Table 2 and the Supporting Information]. Thus, the occurrence of SOC between S_1 and a triplet state with at least partial $n-\pi^*$ character can be excluded as the origin for the increase of the intersystem crossing rate upon N substitution.

The SOC between $\pi-\pi^*$ states in *coplanar* molecules gives rise to very small values, on the order of 0.04−0.05 meV.[51] Because $\pi-\pi^*$ states are antisymmetric with respect to the mirror plane that contains all atoms, only the "out-of-plane" component L_z of the angular momentum operator L gives rise to a nonzero SOC. All major contributions to the associated SOC matrix elements, which can be broken down into contributions from one- and two-center integrals, either nearly cancel each other or vanish exactly, respectively.[52−54] In a nonplanar aromatic molecule, SOC between two $\pi-\pi^*$ states increases with respect to that in coplanar molecules, as the removal of the mirror-plane symmetry allows nonvanishing matrix elements associated with *each* L component. Moreover, the matrix elements become sensitive to the spatial extension of the molecular wavefunctions in the out-of-plane direction and can, as a result, reach values of 0.3 meV.

The SOC matrix elements between S_1 and T_n states strongly depend on the nature of the final triplet state, as seen from Figure 5. This behavior can be rationalized on the basis of the symmetry selection rules pertaining to SOC,[53−55] even though, strictly speaking, the monoaza-H5 molecules do not exhibit any point-group symmetry; their deviation from the C_2 symmetry of the reference H5 molecule is, however, sufficiently small to recognize the *symmetry parentage* (A or B type) in the electronic states of the substituted molecules. For a given triplet state, the *degree* of mixing of A- and B-type wavefunctions depends on the nitrogen position, which, as discussed above, impacts the deviation from planarity, given by the dihedral angle δ. The larger the mixing, the smaller the SOC from S_1 (which is A type) to a predominantly B-type triplet state and the larger the SOC to a predominantly A-type T state. As an illustration, the evolution of SOC for the S_1−T_5 pair as a function of nitrogen position is shown in Figure 6 in comparison to δ; the inverse of δ is plotted because the SOC increases with decreasing δ because of the A parentage of S_1 and the B parentage of T_5.

The spin−orbit couplings between T_1 and the singlet manifold and between S_0 and the triplet manifold are required to determine the transition dipole moment associated with the T_1−S_0 transition. Because the T_1 triplet state has $\pi-\pi^*$ character, the strongest SOC to T_1 occurs with those S_n states carrying considerable $n-\pi^*$ admixture; for such pairs, we find SOC values of ca. 0.3−0.5 meV (up to 1.5 meV in 6-aza-H5). The T_1−S_n SOC matrix elements with $\pi-\pi^*$ singlet states, on the

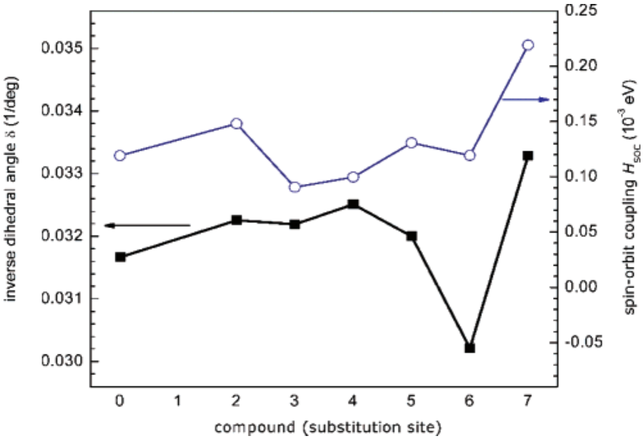

Figure 6. Evolution of the INDO/CIS spin−orbit couplings (open circles) between S_1 and T_5 in comparison to the dihedral angle δ (solid squares), as a function of the nitrogen substitution site in monoaza[5]-helicenes. The site index 0 is associated with the pure hydrocarbon [5]helicene.

other hand, do not exceed 0.35 meV. The SOC observed between S_0−T_n pairs is, in analogous manner, largely affected by the nature of the respective triplet state and can reach values up to 1 meV.

(b) Franck−Condon-Weighted Density of States. To make the connection from spin−orbit coupling to intersystem crossing, we now turn to a discussion of the impact of the Franck−Condon-weighted density of states (see eq 10). The calculation of the FCWD was based on a detailed analysis of the vibrational coupling between S_1 and the low-energy triplet states using their AM1/CI-optimized geometries. We found strongly coupled modes in the range $\hbar\omega = 1400{-}1650$ cm^{-1} that effectively act as one single mode $\hbar\omega_{\rm eff}$. The associated Huang−Rhys factor S was evaluated to be on the order of 0.3, which is comparable to the Huang−Rhys factor related to the $S_0 \rightarrow T_1$ transition. However, we showed earlier[23] that AM1/CI geometries lead to an underestimation of the vibrational coupling in monoazahelicenes, whereas DFT geometries result in S factors of 0.8−0.9, which describe the phosphorescence spectra very well.[23] Therefore, we conducted the modeling of the FCWD with an effective high-frequency vibration $\hbar\omega_{\rm eff} = 1600$ cm^{-1} with $S = 0.9$ and $S = 0.3$. We note that the contributions from low-frequency modes and the solvent-induced relaxation energy were taken into account in a classical fashion by combining them into the parameter λ (Marcus reorganization energy); λ was set to realistic values of $\lambda = 0.1{-}0.2$ eV. (We also explored the impact of significantly smaller and larger λ values.[56])

Figure 7 provides a comparison the evolution of the FCWD for a given λ with respect to the triplet energies relative to S_1. It is immediately seen that the FCWD switches off the strong S_1−T_1 SOC channel entirely, because of the very large S_1−T_1 energy difference. For reasonable λ values of 0.1 and 0.2 eV, T_5 contributes to ISC, whereas the contributions of T_6 or T_7 are very sensitive to the exact choice of λ (and the Huang−Rhys factor S). Subtle differences in the S_1−T_n energy offsets create a significant molecule-dependent mixing of all SOC channels, which actually blurs the N-site dependence affecting the individual SOC channels.

(c) Intersystem Crossing. As observed for $k^{\rm S}_{\rm rad}$, the $k_{\rm ISC}$ rates are dependent on the substitution site, with $k_{\rm ISC}$ presenting its maximum value for 6-aza-H5 ($k_{\rm ISC} = 3.18 \times 10^8$ s^{-1}) and its minimum value for 5-aza-H5 ($k_{\rm ISC} = 1.79 \times 10^8$ s^{-1}).

As indicated earlier, because of the energetic proximity of S_1 and S_2 (cf. Table 2), the calculated intersystem crossing rates collected in Table 4 are sums over the individual, Boltzmann-weigthed ISC rates $k^{\rm S_1}_{\rm ISC}$ and $k^{\rm S_2}_{\rm ISC}$, each calculated with eq 8. We find that the contribution to ISC from S_2 is negligible at 77 K. From Table 4, it is seen that the maximum value is $k_{\rm ISC} = 2.08 \times 10^9$ s^{-1} ($\lambda = 0.1$ eV) for position 6, which is consistent with the measured ISC rates along the series. In full agreement with experiment (Table 3), the derived $k_{\rm ISC}$ rates are more than 1 order of magnitude larger than the calculated fluorescence decay rates $k^{\rm S}_{\rm rad}$ (Table 4). Variation of the Huang−Rhys factor S between 0.3 and 0.9 does not affect the trend among the $k_{\rm ISC}$ rates calculated for 77 K. However, as seen from Table 4, the trend strongly depends on the actual value of λ, independent of the considered temperature. In Figure 8b, we compare the calculated ISC rates at 77 K for $\lambda = 0.1$ and 0.2 eV with the measured rates. Overall, the trends throughout the series are best described when a moderate $\lambda = 0.1$ eV value is assumed.

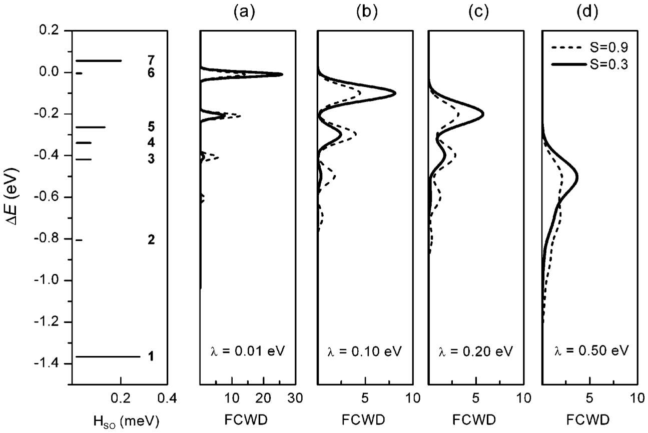

Figure 7. Franck−Condon-weighted density of states (FCWD), eq 10, as a function of the energy offset ΔE for an effective vibrational mode at 1600 cm^{-1}, for two Huang−Rhys factors S, and for various reorganization energies λ ($T = 77$ K). For comparison, the energetic positions of the triplet states T_n (labeled $n = 1{-}7$) with respect to S_1 in H5 are indicated together with the computed SOC values (left panel).

Below, we discuss, with the help of the λ-dependent FCWD values, the SOC channels that actively contribute to the calculated ISC. The FCWD essentially reduces the triplet states to T_4−T_6, which are amenable to ISC with S_1; with increasing energy of the high-frequency effective vibrational mode chosen, the T_3 state can also weakly couple to S_1. For $\lambda = 0.2$ eV, T_5 has the largest overlap with S_1 and, therefore, provides the ISC channel with the largest relative FC weight; the resulting intersystem crossing rates for the monoazahelicenes are shown in Figure 8a and Table 4. With the largest contribution to ISC arising mainly from the S_1−T_5 channel (which clearly dominates all other channels except those for 3-aza- and 6-aza-H5), $k_{\rm ISC}$ becomes sensitive to the *inverse of the dihedral angle* δ, which is inherited from the characteristics of the S_1−T_5 SOC (compare Figures 8a and 6). When the value of λ is reduced to 0.1 eV, the relative weight of T_5 (given by the FCWD value) is reduced in favor of larger overlaps of T_4 and T_6 with S_1 as a result of which the total intersystem crossing rates are determined by the SOC to T_4, T_5, and T_6. With the stronger involvement of T_6 for reorganization energy $\lambda = 0.1$ eV, the $k_{\rm ISC}$ values for 6-aza-H5 and 7-aza-H5 become, because of their large associated SOC, significantly increased (Figure 8a). As a consequence, 6-aza-H5 acquires the largest ISC rate in the series, as seen among the measured ISC rates as well (Figure 8b). Quantitatively, the theoretical predictions overestimate $k_{\rm ISC}$ by an order of magnitude. This deviation might be attributable to a possibly non-negligible back-transfer rate $k_{\rm T_n \rightarrow S_1}$, which is not taken into account in our model, because we assume that ISC is followed

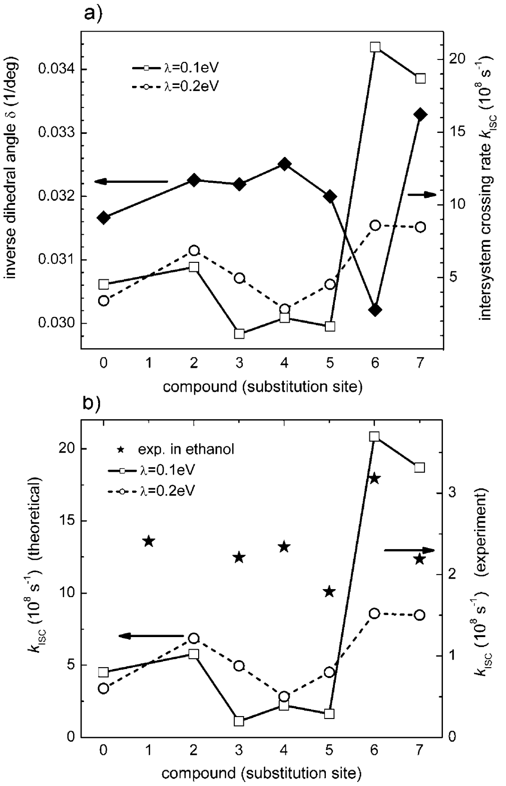

Figure 8. (a) Evolution of the intersystem crossing rate k_{ISC} (open symbols) estimated from eq 10 at $T = 77$ K in comparison to the inverse dihedral angle δ (solid diamonds) as a function of the nitrogen substitution site in monoaza[5]helicenes, for reorganization energies $\lambda = 0.1$ and 0.2 eV (effective high-frequency vibration $\hbar\omega = 1600$ cm^{-1}, $S = 0.9$). (b) Comparison of experimental ISC rates to theoretical ISC rates calculated from eq 10 using different reorganization energies λ ($\hbar\omega = 1600$ cm^{-1}, $S = 0.9$). The site index 0 is associated with the pure hydrocarbon [5]helicene.

TABLE 5: Phosphorescence Lifetime τ_{tot}^{T} and Phosphorescence Decay Rate k_{tot}^{T} (measured at 77 K in Ethanol) and Calculated Spontaneous Radiative Decay Rate k_{rad}^{T} for Monoazahelicences

	experiment		INDO/CIS
compound	τ_{tot}^{T} (s)	k_{tot}^{T} (s^{-1})	k_{rad}^{T} (s^{-1})
H5	2.48	0.40	0.97
1-aza-H5	1.88	0.53	1.02
2-aza-H5	1.80	0.56	0.95
3-aza-H5	2.16	0.46	0.53
4-aza-H5	1.82	0.55	1.11
5-aza-H5	1.96	0.51	1.66
6-aza-H5	0.91	1.10	3.01
7-aza-H5	1.55	0.65	1.06

by instantaneous relaxation from T_n into T_1. A second source of deviation might be the systematic overestimation of the SOC expectation values (because inaccuracies in the FCWD estimates would actually yield smaller deviations).

(d) Phosphorescence Lifetimes. The total phosphorescence lifetime measured in the monoaza[5]helicenes is in the range 1−2.5 s (Table 5) at 77 K. H5 exhibits the largest lifetime ($\tau_{tot}^{T} = 2.5$ s), whereas 6-aza-H5 exhibits the shortest one ($\tau_{tot}^{T} = 0.91$ s). The introduction of a nitrogen atom into the carbon backbone causes a drop in the lifetime, which was found to be significantly dependent on the substitution position. The total lifetimes are temperature-independent below 100 K (all non-radiative contributions associated with an activation energy being then frozen in).

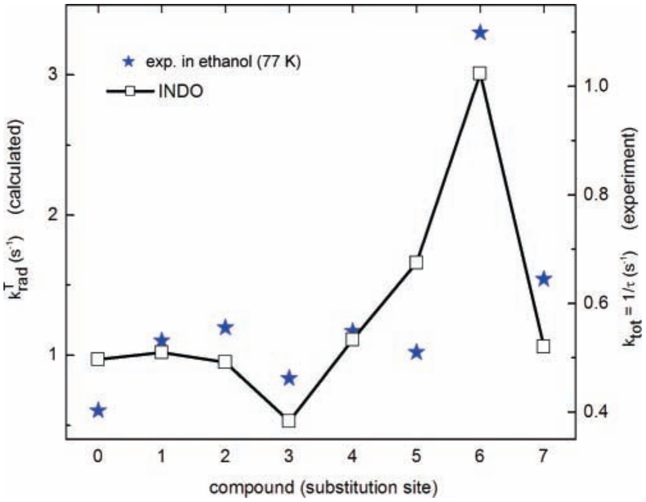

Figure 9. Phosphorescence decay rate k_{tot}^{T} and calculated radiative decay rate k_{rad}^{T} as a function of the nitrogen substitution site in monoaza[5]helicenes.

To estimate the triplet radiative lifetimes, we assumed that phosphorescence originates from the thermally relaxed T_1 state. The *radiative* decay rates k_{rad}^{T} were calculated by plugging into eq 7 the SOC values and transition dipole moments computed within the singlet and triplet manifolds at the T_1 equilibrium geometry. The calculated rates agree remarkably well with the total decay rates obtained experimentally (Table 5), both in terms of the order of magnitude (deviations within a factor of 3) and in terms of the overall trends (Figure 9).

It is clear from eq 7 that terms with either (a) a large transition dipole moment or (b) a large SOC matrix element will contribute most significantly to the overall $\mu_{T_1 \rightarrow S_0}$ transition dipole moment. The largest transition dipole moments are associated with states of almost pure $\pi-\pi^*$ character.

Thus, factors (a) and (b) can be exploited simultaneously when T_1 (S_0) couples to a strongly dipole-allowed singlet (triplet) state that is predominantly of $\pi-\pi^*$ character but also features a significant $n-\pi^*$ admixture. In each of the monoaza[5]helicene molecules, we find several S_n and T_n states of such character and large associated transition dipole moments ($\vec{\mu}_{S_n \rightarrow S_0}$ and $\vec{\mu}_{T_n \rightarrow T_1}$). In contrast to ISC from S_1, which is dominated by only a few SOC channels, all of these S_n and T_n states enter the summation in eq 7 with large terms that partially cancel each other, causing the calculated decay rate of 3-aza-H5 to drop below the k_{rad}^{T} value of the nitrogen-free H5.

V. Conclusions

The introduction of a nitrogen atom into the carbon backbone of [5]helicene has been shown to induce large variations in the luminescence properties, which depend strongly on the nitrogen substitution site. Both the intersystem crossing rates and the radiative phosphorescence decay rates are enhanced with respect to [5]helicene. In the case of ISC, this enhancement is directly related to the spin−orbit coupling whose expectation values are sensitive to the *degree of nonplanarity.* The deviation from planarity, reflected by the inner dihedral angle δ, can be tuned by the substitution site of the nitrogen atom. As was demonstrated with the help of monoaza[5]helicenes as model systems, introduction of a heteroatom into a nonplanar conjugated molecule can affect its ISC behavior not only by introducing lower-lying $n-\pi^*$ transitions (relevant for small molecules), but also by changing its deviation from planarity, an effect that is expected to dominate the former for larger compounds.

The observed increase in radiative phosphorescence decay rates with respect to H5 originates from the presence of states of partial $n-\pi^*$ character among the higher excited singlet and triplet states. Such states lead to a large SOC to T_1 and S_0; when these particular singlet (triplet) states exhibit a large transition dipole moment to S_0 (T_1) (inherited from their predominant $\pi-\pi^*$ character), considerable oscillator strength can be acquired for the T_1-S_0 transition. The calculated phosphorescence decay rates are in remarkable agreement with experimental data.

Acknowledgment. The authors are indebted to J. Reimers for most kindly providing his DUSHIN program. The work at the Georgia Institute of Technology was partly supported by the National Science Foundation (Grant CHE-0342321 and CRIF Award 04-43564) and the Office of Naval Research. The work at Milano-Bicocca University was supported by the Italian MURST (Firb RBAU01N449 Project). D.B. and J.C. are Research Fellows of the Belgian National Research Science Foundation (FNRS). The work in Beijing was supported by NSFC (Grants 20420150034, 20421101, and 10425420).

Supporting Information Available: Tables of energies and comparison between measured and simulated absorption spectra. This material is available free of charge via the Internet at http://pubs.acs.org.

References and Notes

(1) Sapir, M.; Vander Donckt, E. *Chem. Phys. Lett.* **1975**, *36*, 108−110.

(2) Beljonne, D.; Shuai, Z.; Pourtois, G.; Brédas, J. L. *J. Phys. Chem. A* **2001**, *105*, 3899−3907.

(3) Nijegorodov, N. I.; Downey W. S. *J. Phys. Chem.* **1994**, *98*, 5639−5643.

(4) Furche, F.; Ahlrichs, R.; Wachsmann, C.; Weber, E.; Sobanski, A.; Vögtle, F.; Grimme S. *J. Am. Chem. Soc.* **2000**, *122*, 1717−1724.

(5) Lebon, F.; Longhi, G.; Gangemi, F.; Abbate, S.; Priess, J.; Juza, M.; Bazzini, C.; Caronna, T.; Mele, A. *J. Phys. Chem. A* **2004**, *108*, 11752−11761.

(6) Bazzini, C.; Brovelli, S.; Caronna, T.; Gambarotti, C.; Giannone, M.; Macchi, P.; Meinardi, F.; Mele, A.; Panzeri, W.; Recupero, F.; Sironi, A.; Tubino R. *Eur. J. Org. Chem.* **2005**, 1247−1257.

(7) Caronna, T.; Gabbiadini, S.; Mele, A.; Recupero, F. *Helv. Chim. Acta* **2002**, *85*, 1−8.

(8) (a) Clar, E.; Zander, M. *Arom. Kohlenwasserst.* **1956**, *89*, 749−762. (b) Clar, E. *Polycyclic Hydrocarbons*; Academic Press: London, 1964; pp 277−280.

(9) Palewska, K.; Ruziewicz, Z.; Chojnacki, H. *Chem. Phys.* **1992**, *161*, 437−445.

(10) Palewska, K.; Chojnacki H. *J. Mol. Struct.* **2002**, *611*, 23−32.

(11) Palewska, K.; Chojnacki H. *Mol. Cryst. Liq. Cryst.* **1993**, *229*, 31−36.

(12) O'Dwyer, M. F.; Ashraf El-Bayoumi, M.; Strickler, J. *J. Chem. Phys.* **1962**, *36*, 1395−1396.

(13) Kim, S. S.; Weissman, S. I. *J. Am. Chem. Soc.* **1969**, *101*, 5863−5864.

(14) Weigang, O. E., Jr.; Turner, J. A.; Trouard, P. A. *J. Chem. Phys.* **1966**, *45*, 1126−1134.

(15) Lower, S. K.; El-Sayed, M. A. *Chem. Rev.* **1966**, *66*, 199−241.

(16) Gropper, H.; Dörr, F. *Ber. Bunsen-Ges. Phys. Chem.* **1963**, *67*, 46.

(17) El-Sayed, M. A.; Brewer, R. G. *J. Chem. Phys.* **1963**, *39*, 1623.

(18) Lim, E. C.; Yu, J. M. H. *J. Chem. Phys.* **1966**, *45*, 4742.

(19) (a) Lim, E. C.; Yu, J. M. H. *J. Chem. Phys.* **1967**, *47*, 3270. (b) Lim, E. C.; Yu, J. M. H. *J. Chem. Phys.* **1968**, *49*, 3878. (c) Li, R.; Lim, E. C. *J. Chem. Phys.* **1972**, *57*, 605.

(20) (a) Masetti, F.; Mazzucato, U.; Birks, J. B. *Chem. Phys.* **1975**, *9*, 301−306. (b) Shatrov, V. D.; Kuznetsov, V. S.; Andreev, O. M.; Korshunov, L. I.; Mikhailov, Yu. A.; Batekha, I. G.; El'tsov, A. V. *Zh. Prikl. Spektrosk.* **1978**, *29*, 51−55. (c) Korshunov, L. I.; Shatrov, V. D.; Kuznetsov, V. S.; Rachek, V. F.; Mikhailov, Yu. A.; Batekha, I. G.; El'tsov, A. V. *Zh. Prikl. Spektrosk.* **1980**, *33*, 700−705.

(21) (a) Dierksen, M.; Grimme S. *J. Chem. Phys.* **2004**, *120*, 3544−3554. (b) Dierksen, M.; Grimme, S. *J. Phys. Chem. A* **2004**, *108*, 10225−10237.

(22) (a) Fedorov, D. G.; Koseki, S.; Schmidt, M. W.; Gordon, M. S. *Int. Rev. Phys. Chem.* **2003**, *22*, 551−592. (b) Aikens, C. M.; Gordon, M. S. *J. Phys. Chem A* **2003**, *107*, 104−114. (c) Christiansen, O.; Gauss, J.; Schmimmelpfennig, B. *Phys. Chem. Chem. Phys.* **2000**, *2*, 965−971. (d) Kleinschmidt, M.; Tatchen, J.; Marian, C. M. *J. Comput. Chem.* **2002**, *23*, 824−833. (e) Minaev, B. *Spectrochim. Acta A* **2004**, *60*, 3213−3224. (f) Minaev, B.; Ågren, H. *Chem. Phys.* **2005**, *315*, 215−239. (g) Minaev, B.; Jansson, E.; Ågren, H.; Schrader, S. *J. Chem. Phys.* **2006**, *125*, 234704. (h) Jansson, E.; Minaev, B.; Schrader, S.; Ågren, H. *Chem. Phys.* **2007**, *333*, 157−167. (i) Fabian, *J. Theor. Chem. Acc.* **2001**, *106*, 199−217.

(23) Schmidt, K.; Brovelli, S.; Coropceanu, V.; Brédas, J. L.; Bazzini, C.; Caronna, T.; Tubino, R.; Meinardi, F. *J. Phys. Chem. A* **2006**, *110*, 11018−11024.

(24) Material Details: Quinine Sulfate, Fluorescence; NIST Standard Reference Material SRM# 936a; available at www.nist.gov/srm.

(25) Grellmann, K.-H.; Hentzschel, P.; Wismontski-Kittel, T.; Fischer, E. *J. Photochem.* **1979**, *11*, 197−213.

(26) Runge, E.; Gross, E. K. U. *Phys. Rev. Lett.* **1984**, *52*, 997−1000.

(27) Gross, E. K. U.; Kohn, W. *Adv. Quantum Chem.* **1990**, *21*, 255−291.

(28) Gross, E. K. U.; Dobson, J. F.; Petersilka, M. *Top. Curr. Chem.* **1996**, *181*, 81−172.

(29) Becke, A. D. *J. Chem. Phys.* **1993**, *98*, 5648−5652.

(30) Schäfer, A.; Horn, H.; Ahlrichs, R. *Chem. Phys. Lett.* **1992**, *97*, 2571−2577.

(31) (a) Bauernschmitt, R.; Ahlrichs, R. *Chem. Phys. Lett.* **1996**, *256*, 454−464. (b) Bauernschmitt, R.; Ahlrichs, R. *Chem. Phys. Lett.* **1997**, *264*, 573−578. (c) Furche, F.; Ahlrichs, R. *J. Chem. Phys.* **2002**, *117*, 7433−7447; for the current version, see www.turbomole.de.

(32) Dewar, M. J. S.; Zoebisch, E. G.; Healy, E. F.; Stewart, J. J. P. *J. Am. Chem. Soc.* **1985**, *107*, 3902−3909.

(33) *AMPAC 8*; Semichem, Inc.: Shawnee, KS, 1992−2004.

(34) Ridley, J.; Zerner, M. C. *Theor. Chim. Acta* **1973**, *32*, 111−134.

(35) Ohno, K. *Theor. Chem. Acta* **1964**, *2*, 219−227. Klopman, G. *J. Am. Chem. Soc.* **1964**, *86*, 4550−4557.

(36) Mataga, N.; Nishimoto, K. *Z. Phys. Chem.* **1957**, *13*, 140−157.

(37) In our systems, the S_1 singlet state energies computed with INDO/CIS (Mataga−Nishimoto) compare well to experiment, but the T_1 triplet energies are up to 1 eV below the experimental values.

(38) Henry, B. R.; Siebrand, W. *J. Chem. Phys.* **1969**, *51*, 2396−2405.

(39) Lawetz, V.; Orlandi, G.; Siebrand, J. W. *Chem. Phys.* **1972**, *56*, 4058−4072.

(40) Robinson, G. W.; Frosch, R. P. *J. Chem. Phys.* **1963**, *38*, 1187−1203.

(41) Brédas, J. L.; Beljonne, D.; Coropceanu, V.; Cornil, J. *Chem. Rev.* **2004**, *104*, 4971−5003.

(42) Reimers, J. *J. Chem. Phys.* **2001**, *115*, 9103−9109.

(43) Grimme, S.; Peyerimhoff, S. D. *Chem. Phys.* **1996**, *204*, 411−417.

(44) Kuroda, R. *J. Chem. Soc., Perkin Trans. 2* **1982**, 789−794.

(45) Sironi, A. CNR CSSMTBO, Milan, Italy. Crystal structure of 1-aza-H5. Private communication, 2005.

(46) Buss, V.; Kolster, K. *Chem. Phys.* **1996**, *203*, 309−316.

(47) Birks, J. B. *Photophysics of Aromatic Molecules*; Wiley: London, 1970.

(48) Brown, A.; Kemp, C. M.; Mason, S. F. *J. Chem. Soc. A* **1971**, 751−755.

(49) (a) Buenker, R. J.; Peyerimhoff, S. D. *Theor. Chim. Acta* **1974**, *35*, 33. (b) Tavan, P.; Schulten, K. J. *Chem. Phys.* **1986**, *85*, 6602. (c) Shuai, Z.; Beljonne, D.; Brédas, J. L. *J. Chem. Phys.* **1992**, *97*, 1132. (d) Zheng, S.; Leclercq, A.; Fu, J.; Beverina, L.; Padilha, L. A.; Zojer, E.; Schmidt, K.; Barlow, S.; Luo, J.; Jiang, S.-H.; Jen, A. K.-Y.; Yi, Y.; Shuai, Z.; Van Stryland, E. W.; Hagan, D. J.; Brédas, J.-L.; Marder, S. R. *Chem. Mater.* **2007**, *19*, 432−442. (e) The 10 highest occupied and 10 lowest unoccupied molecular orbitals were active in the MRDCI procedure for single and double excitations relative to the reference determinants. The SCF determinant, three singly excited determinants (HOMO → LUMO, HOMO − 1 → LUMO, HOMO → LUMO + 1), and the doubly excited determinant with both electrons promoted from the HOMO to the LUMO (HOMO, HOMO → LUMO, LUMO) were chosen as reference determinants.

(50) See, for example, (a) Zojer, E.; Beljonne, D.; Kogej, T.; Vogel, H.; Marder, S. R.; Perry, J. W. *J. Chem. Phys.* **2002**, *116*, 3646−3658. (b) Engel, E.; Schmidt, K.; Beljonne, D.; Brédas, J.-L.; Assa, J.; Fröb, H.; Leo, K.; Hoffmann, M. *Phys. Rev. B* **2006**, *73*, 245216.

(51) Hameka, H.; Oosterhoff, L. *Mol. Phys.* **1958**, *1*, 358−371.

(52) El-Sayed, M. A. *J. Chem. Phys.* **1963**, *38*, 2834−2838.

(53) McClure, D. S. *J. Chem. Phys.* **1949**, *17*, 665−666.

(54) Weissman, S. I. *J. Chem. Phys.* **1950**, *18*, 232−233.

(55) McClure, D. S. *J. Chem. Phys.* **1952**, *10*, 682−686.

(56) Because no significant charge redistribution is observed upon relaxation from S_1 into T_1 (corresponding state dipole moment changes less than 0.6 D), we expect a relaxation energy not larger than 0.2 eV).